CrossMark

electronic reprint

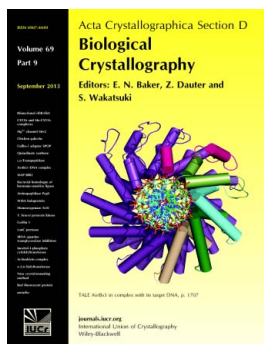# Structural basis of high-order oligomerization of the cullin-3 adaptor SPOP

Laura K. van Geersdaele, Mark A. Stead, Christopher M. Harrison, Stephen B. Carr, Helen J. Close, Gareth O. Rosbrook, Simon D. Connell and Stephanie C. Wright

Acta Crystallographica Section D: Biological Crystallography welcomes the submission of papers covering any aspect of structural biology, with a particular emphasis on the structures of biological macromolecules and the methods used to determine them. Reports on new protein structures are particularly encouraged, as are structure–function papers that could include crystallographic binding studies, or structural analysis of mutants or other modified forms of a known protein structure. The key criterion is that such papers should present new insights into biology, chemistry or structure. Papers on crystallographic methods should be oriented towards biological crystallography, and may include new approaches to any aspect of structure determination or analysis. Papers on the crystallization of biological molecules will be accepted providing that these focus on new methods or other features that are of general importance or applicability.

Crystallography Journals Online is available from journals.iucr.org

Structural basis of high-order oligomerization of the cullin-3 adaptor SPOP

Laura K. van Geersdaele,[a]‡
Mark A. Stead,[a]‡ Christopher M.
Harrison,[a] Stephen B. Carr,[b]
Helen J. Close,[a] Gareth O.
Rosbrook,[a] Simon D. Connell[c]
and Stephanie C. Wright[a]*

[a]School of Biology, University of Leeds,
Leeds LS2 9JT, England, [b]Research Complex at
Harwell, Rutherford Appleton Laboratory,
Harwell Oxford, Didcot OX11 0FA, England,
and [c]School of Physics and Astronomy,
University of Leeds, Leeds LS2 9JT, England

‡ LKvG and MAS contributed equally to this
work.

Correspondence e-mail: s.c.wright@leeds.ac.uk

Protein ubiquitination in eukaryotic cells is mediated by diverse E3 ligase enzymes that each target specific substrates. The cullin E3 ligase complexes are the most abundant class of E3 ligases; they contain various cullin components that serve as scaffolds for interaction with substrate-recruiting adaptor proteins. SPOP is a BTB-domain adaptor of the cullin-3 E3 ligase complexes; it selectively recruits substrates via its N-terminal MATH domain, whereas its BTB domain mediates dimerization and interactions with cullin-3. It has recently been recognized that the high-order oligomerization of SPOP enhances the ubiquitination of substrates. Here, a dimerization interface in the SPOP C-terminus is identified and it is shown that the dimerization interfaces of the BTB domain and of the C-terminus act independently and in tandem to generate high-order SPOP oligomers. The crystal structure of the dimeric SPOP C-terminal domain is reported at 1.5 Å resolution and it is shown that Tyr353 plays a critical role in high-order oligomerization. A model of the high-order SPOP oligomer is presented that depicts a helical organization that could enhance the efficiency of substrate ubiquitination.

1. Introduction

Ubiquitination is a highly regulated post-translational modification that targets proteins for degradation by the 26S proteasome and also plays nonproteolytic roles in controlling protein–protein interactions, subcellular localization and enzymatic activity (reviewed in Komander & Rape, 2012). It is carried out by an enzyme cascade in which ubiquitin is first transferred from an E1 activating enzyme onto an E2 conjugating enzyme. An E3 ubiquitin–protein ligase then catalyses the transfer of ubiquitin from the E2 enzyme to the substrate. E3 ligases of the HECT (**h**omologous to the **E**6AP **c**arboxyl **t**erminus) domain family contain an active-site cysteine that forms an obligate thioester intermediate with ubiquitin; in contrast, the RING (**r**eally **i**nteresting **n**ew **g**ene) finger E3 ligases do not form a catalytic intermediate with ubiquitin, but instead act to bring the substrate and E2 enzyme into close proximity to facilitate ubiquitin transfer. There are approximately 30 HECT-domain E3s and over 600 RING-finger E3s in mammals, and this diversity allows the independent ubiquitination of different substrates. The regulated ubiquitination of specific proteins is critical for fundamental biological processes such as the cell cycle and apoptosis, and alterations in ubiquitination pathways have been implicated in many human disease states (reviewed in Nalepa et al., 2006; Petroski, 2008).

The cullin–RING E3 ligase complexes are multisubunit enzymes that together constitute the largest subclass of RING-finger E3 ligases. They contain a cullin component

(Cul1, Cul2, Cul3, Cul4a, Cul4b, Cul5 or Cul7) together with various adaptor modules that selectively recognize specific substrates. The N-termini of the cullins interact with the adaptors, whereas their C-termini interact with a RING-domain protein that in turn recruits the E2 enzyme (reviewed in Zimmerman *et al.*, 2010). The Cul3 adaptors (reviewed in Pintard *et al.*, 2004) recruit substrates *via* domains such as Kelch or MATH (**m**ephrin **a**nd **T**RAF **h**omology), and they interact with cullin *via* their BTB [**b**ric-à-brac, **t**ramtrack and **b**road complex; also known as POZ (**po**xvirus and **z**inc finger)] domain, a versatile protein–protein interaction domain that is also found in zinc-finger transcription factors (reviewed in Stogios *et al.*, 2005).

SPOP (**s**peckle-type **PO**Z **p**rotein) is a MATH-BTB-type Cul3 adaptor that regulates cell proliferation and development (Nagai *et al.*, 1997). The MATH domain of SPOP interacts with serine/threonine-rich degrons in target proteins (Zhang *et al.*, 2009; Zhuang *et al.*, 2009) that include the apoptotic regulator Daxx (Kwon *et al.*, 2006), the steroid receptor co-activator SRC-3 (Li *et al.*, 2011) and the variant histone protein MacroH2A (Takahashi *et al.*, 2002). SPOP has been implicated both as an oncogene (Liu *et al.*, 2009; Kim *et al.*, 2011) and as a tumour suppressor (Barbieri *et al.*, 2012; Li *et al.*, 2011) in human cancer.

Substrate ubiquitination is enhanced by the self-association of various E3 ligase components (reviewed in Zimmerman *et al.*, 2010), and structures of parts of the Cul3 adaptors SPOP and gigaxonin (Zhuang *et al.*, 2009) revealed BTB-mediated dimers that resemble the BTB-domain dimers found in transcription factors. Many SPOP substrates contain multiple weak degrons that may simultaneously bind to the two MATH domains of an SPOP dimer (Zhang *et al.*, 2009; Zhuang *et al.*, 2009), thereby enhancing ubiquitination. Although the dimerization properties of BTB domains have been well characterized, it is recognized that higher-order oligomerization is important for the activities of several BTB proteins (see, for example, Espinás *et al.*, 1999), and it has recently been shown that the high-order oligomerization of SPOP leads to enhanced substrate ubiquitination by Cul3 E3 ligase complexes (Errington *et al.*, 2012); the structural basis of these important high-order associations is unknown. Here, we identify a novel dimerization interface in the C-terminus of SPOP that, in concert with the BTB domain, directs the formation of high-order oligomers. The X-ray crystal structure of the SPOP C-terminal domain enables us to propose a model of the high-order SPOP oligomer that reveals the mechanism by which substrate ubiquitination is enhanced by adaptor oligomerization.

2. Materials and methods

2.1. Cloning

A cDNA encoding human SPOP residues 1–374 was amplified by PCR from a human placental cDNA library. SPOP fragments were cloned into pGEX-6P-1 (GE Healthcare) for bacterial expression of GST-fusion proteins. Point mutations and deletions were generated by PCR using Phusion High-Fidelity DNA polymerase (Thermo Scientific). The SPOP proteins expressed in bacteria were SPOP$^{169–374}$, SPOP$^{169–334}$, SPOP$^{169–296}$, SPOP$^{169–359}$, SPOP$^{169–355}$, SPOP$^{169–344}$, SPOP$^{169–374 \ Y353E}$ and SPOP$^{270–374 \ L273D \ L282D \ L285K}$.

2.2. Protein expression and purification

GST-SPOP proteins were expressed in *Escherichia coli* BL21 (DE3) pLysS. Recombinant proteins were induced with 0.1 mM IPTG at 289 K. Bacteria were lysed using a cell disrupter (Constant Systems), the fusion proteins were bound to glutathione-Sepharose 4B (GE Healthcare) and the N-terminal GST tag was removed by cleavage with PreScission protease in 20 mM Tris–HCl, 75 mM NaCl, 5 mM DTT pH 7.5. SPOP proteins were further purified by size-exclusion chromatography on a Superdex 75 HiLoad 26/60 column (GE Healthcare) in 20 mM Tris–HCl, 150 mM NaCl, 5 mM DTT, 5% glycerol pH 8.6. Protein preparations for crystallization were concentrated using Vivaspin centrifugal concentrators (Sartorius). Selenomethionine-substituted GST-SPOP was expressed in *E. coli* B834 (DE3) pLysS; the cells were cultured in minimal medium in which the methionine was substituted by 45 µg ml^{-1} L-selenomethionine.

2.3. Crystallization

Crystals of native SPOP$^{270–374 \ L273D \ L282D \ L285K}$ were grown at 291 K by hanging-drop vapour diffusion against 26% PEG 1500, 0.1 M imidazole pH 6.5, 0.1 M CaCl$_2$, 7% 2-propanol; drops were prepared by mixing 2 µl reservoir solution with 1 µl 8 mg ml^{-1} protein solution. Crystals grew to average dimensions of 150 × 25 × 25 µm within 5 d. Crystals of selenomethionine-substituted SPOP$^{270–374 \ L273D \ L282D \ L285K}$ were grown by hanging-drop vapour diffusion against 29% PEG 1500, 0.1 M imidazole pH 6.5, 0.1 M CaCl$_2$, 7% 2-propanol. Crystals of SPOP$^{169–374 \ Y353E}$ were grown at 291 K by sitting-drop vapour diffusion against 32% PEG 3350, 17% 2-propanol, 0.1 M Tris–HCl pH 8.5; drops were prepared by mixing 2 µl reservoir solution with 2 µl 16 mg ml^{-1} protein solution and crystals grew to average dimensions of 200 × 200 × 15 µm within 2 d. Crystals of SPOP$^{270–374 \ L273D \ L282D \ L285K}$ were cryoprotected by transfer for 30 s into mother liquor supplemented with 20% glycerol before being flash-cooled in liquid nitrogen; crystals of SPOP$^{169–374 \ Y353E}$ were cryoprotected with mother liquor supplemented with 19% ethylene glycol.

2.4. X-ray data collection and structure determination

X-ray data were collected on Diamond Light Source beamlines I02 (native SPOP$^{270–374 \ L273D \ L282D \ L285K}$), I04-1 (selenomethionine-substituted SPOP$^{270–374 \ L273D \ L282D \ L285K}$) and I03 (native SPOP$^{169–374 \ Y353E}$). X-ray data were processed, reduced and scaled using *XDS* (Kabsch, 2010) and *SCALA* (Evans, 2006) or *AIMLESS* using the *xia*2 pipeline (Winter, 2010). The structure of SPOP$^{270–374 \ L273D \ L282D \ L285K}$ was determined by SAD phasing using *SHELXD* (Sheldrick, 2008; Schneider & Sheldrick, 2002) for the heavy-atom

search and *SHELXE* for initial phase estimation and density modification. The phases were combined with native amplitudes and an initial model was built using *ARP/wARP* (Cohen *et al.*, 2008). The structure of SPOP[169–374 Y353E] was solved by molecular replacement using *Phaser* (McCoy *et al.*, 2007) with the human SPOP BTB domain (PDB entry 3htm; chain *A* residues 177–299; Zhuang *et al.*, 2009) and human SPOP CTD (structure of SPOP[270–374 L273D L282D L285K]; residues 300–359) as independent search models. The model was built using *ARP/wARP* (Cohen *et al.*, 2008) and underwent density modification using *Parrot* (Zhang *et al.*, 1997). The models of SPOP[270–374 L273D L282D L285K] and SPOP[169–374 Y353E] underwent several rounds of iterative refinement in *REFMAC*5 (Murshudov *et al.*, 2011) and model building using *Coot* (Emsley *et al.*, 2010). The final models consist of SPOP residues 296–359 (SPOP[270–374 L273D L282D L285K]) and 178–356 (SPOP[169–374 Y353E]). Stereochemistry was analysed with *MolProbity* (Chen *et al.*, 2010). Structure superpositions were calculated using the *SuperPose* server (Maiti *et al.*, 2004) and buried surface areas and residue contacts were obtained using the *PISA* server (Krissinel & Henrick, 2007). Illustrations of protein structures were prepared using *CCP4mg* (McNicholas *et al.*, 2011).

2.5. Chemical cross-linking of purified SPOP proteins

Protein was purified by size-exclusion chromatography in PBS and cross-linked by incubation with 6 m*M* *N*-hydroxysulfosuccinimide, 6 m*M* 1-ethyl-3-(3-dimethylaminopropyl)-carbodiimide hydrochloride for 2 h at 294 K.

2.6. Atomic force microscopy

A freshly cleaved mica surface was incubated for 10 min in 5 m*M* MgCl$_2$, briefly rinsed with deionized water (18.2 MΩ cm^{-1}) and dried in a stream of N$_2$ gas; Mg^{2+} modifies the negatively charged mica surface, thus assisting the binding of SPOP protein, which is also negatively charged at neutral pH. Purified SPOP[169–374] was diluted to 1 μg ml^{-1} in PBS pH 7.4 supplemented with 5 m*M* MgCl$_2$, and the mica surface was incubated for 30 min with 50 μl of the diluted protein. The disc was gently and briefly washed with deionized water (18.2 MΩ cm^{-1}) and dried in a stream of N$_2$ gas.

The sample was imaged using a Multimode 8 atomic force microscope (Bruker) using PPP-NCLR probes (Nanosensors; resonant frequency 170 kHz). Images were acquired in attractive-regime amplitude-modulation tapping mode, operating with small r.m.s. amplitudes of <0.15 V. The images shown are from two independently purified samples of SPOP protein; each batch was imaged at least three times. Data were analysed and processed using *NANOSCOPE ANALYSIS* v.1.40r1 (Bruker).

3. Results

3.1. Crystal structure of the SPOP C-terminal domain

Human SPOP is a 374-residue protein that contains an N-terminal MATH domain (residues 28–166) that recruits substrates and a central BTB domain (residues 177–296) that mediates dimerization and interactions with Cul3 (Fig. 1*a*). The SPOP C-terminus is predicted to contain an α-helical region (residues 298–359) and a basic nuclear localization signal (NLS; residues 365–374), and it has recently been shown that the C-terminus is involved in dynamic high-order oligomerization (Errington *et al.*, 2012). To analyse the oligomerization properties of the SPOP C-terminus, we expressed SPOP[169–374], which contains the BTB domain together with the C-terminus, in *E. coli*. The purified protein eluted as a high-molecular-weight species (>100 kDa) upon size-exclusion chromatography, and chemical cross-linking of the protein produced high-order oligomers (Supplementary Fig. S1*a*[1]). In contrast, the purified BTB domain, SPOP[169–296], was dimeric, as was a protein that contained an incomplete C-terminus (SPOP[169–334]), suggesting that the C-terminal residues 335–374 are required for high-order oligomerization (Supplementary Fig. S1*a*). To study the C-terminus of SPOP in isolation from the BTB domain, we purified SPOP[270–374 L273D L282D L285K], which contains the two C-terminal α-helices (α5 and α6) of the BTB domain together with the entire SPOP C-terminus; the solubility of this protein was increased by the mutation of three surface-exposed hydrophobic residues of α5 and α6. SPOP[270–374 L273D L282D L285K] was dimeric when analysed by size-exclusion chromatography and chemical cross-linking (Supplementary Fig. S1*b*), suggesting that the SPOP C-terminus contains a dimerization interface that is independent of the BTB domain.

To elucidate the mechanism of the high-order oligomerization of SPOP, we determined the X-ray crystal
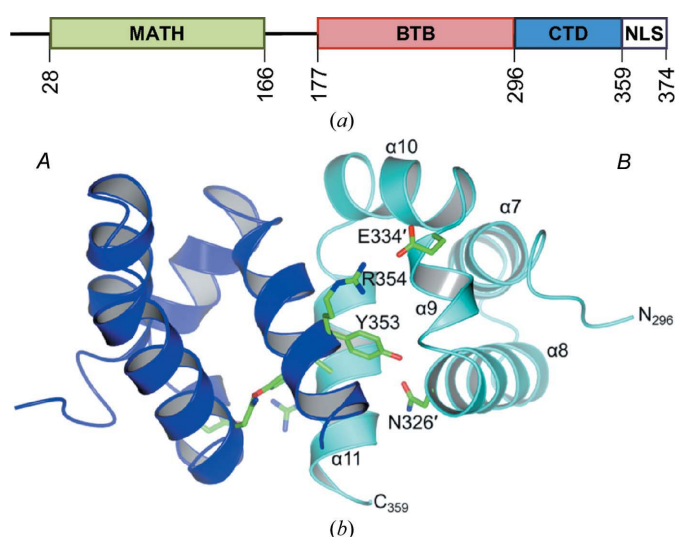

Figure 1
Crystal structure of the SPOP C-terminal domain (CTD). (*a*) Domain organization of human SPOP. (*b*) Cartoon representation of the SPOP CTD dimer. The two chains are coloured blue and cyan. Secondary-structure elements of the *B* chain and interacting residues of the dimerization interface are indicated; residues of the *B* chain are indicated with a prime.

Table 1
Data-collection and refinement statistics.

Values in parentheses are for the highest resolution shell.

	SPOP[270–374 L273D L282D L285K], native	SPOP[270–374 L273D L282D L285K], SeMet	SPOP[169–374 Y353E], native
PDB code	4hs2		4j8z
Crystal parameters			
Space group	$P6_122$	$P6_122$	$C121$
Unit-cell parameters (Å, °)	$a = 57.65, b = 57.65, c = 102.81,$ $\alpha = 90.00, \beta = 90.00, \gamma = 120.00$	$a = 57.58, b = 57.58, c = 102.81,$ $\alpha = 90.00, \beta = 90.00, \gamma = 120.00$	$a = 111.39, b = 71.58, c = 62.22,$ $\alpha = 90.00, \beta = 117.21, \gamma = 90.00$
Data collection			
Resolution (Å)	51.40–1.53 (1.57–1.53)	51.40–2.12 (2.18–2.12)	58.02–2.42 (2.48–2.42)
Wavelength (Å)	0.9795	0.9173	0.9763
R_{merge}† (%)	5.6 (64.7)	18.5 (89.9)	4.4 (34.6)
$R_{p.i.m.}$‡ (%)	1.7 (25.0)	2.9 (15.7)	2.7 (21.6)
$\langle I/\sigma(I)\rangle$	24.2 (3.1)	38.4 (9.0)	17.2 (3.7)
No. of unique reflections	16004 (1143)	6183 (437)	16513 (1207)
Multiplicity	11.6 (8.3)	71.5 (60.1)	3.5 (3.5)
Completeness (%)	99.8 (99.9)	100.0 (100.0)	98.9 (98.1)
Refinement			
Resolution (Å)	27.76–1.53		58.02–2.42
R§ (%)	13.2		20.7
R_{free}¶ (%)	15.1		25.5
R.m.s.d. stereochemistry††			
Bond lengths (Å)	0.011		0.014
Bond angles (°)	1.17		1.58
No. of protein atoms	542		2762
No. of water molecules	62		25
Average B factor (Å²)	16.90		64.28
Ramachandran analysis‡‡ (%)			
Favoured	100.0		97.7
Allowed	0.0		2.3
Disallowed	0.0		0.0

† $R_{merge} = \sum_{hkl}\sum_i |I_i(hkl) - \langle I(hkl)\rangle|/\sum_{hkl}\sum_i I_i(hkl)$, where $I_i(hkl)$ is the integrated intensity of a given reflection and $\langle I(hkl)\rangle$ is the mean intensity of multiple corresponding symmetry-related reflections. ‡ $R_{p.i.m.} = \sum_{hkl}\{1/[N(hkl) - 1]\}^{1/2}\sum_i |I_i(hkl) - \langle I(hkl)\rangle|/\sum_{hkl}\sum_i I_i(hkl)$, where $I_i(hkl)$ is the integrated intensity of a given reflection, $\langle I(hkl)\rangle$ is the mean intensity of multiple corresponding symmetry-related reflections and $N(hkl)$ is the multiplicity of a given reflection. § $R = \sum_{hkl} ||F_{obs}| - |F_{calc}||/\sum_{hkl} |F_{obs}|$, where F_{obs} and F_{calc} are the observed and calculated structure factors, respectively. ¶ R_{free} is as R but calculated using a random 5% of data excluded from refinement. †† R.m.s.d. stereochemistry is the deviation from ideal values. ‡‡ Ramachandran analysis was carried out using *MolProbity* (Chen *et al.*, 2010).

structure of the C-terminus at 1.5 Å resolution. The SPOP[270–374 L273D L282D L285K] dimer crystallized with a monomer in the asymmetric unit; the dimer was revealed from crystallographic symmetry (Table 1, Fig. 1*b* and Supplementary Fig. S2). No electron density was observed for the residues comprising the predicted nuclear localization signal (residues 360–374) and BTB $\alpha5$–$\alpha6$ (residues 270–295), and they were not built in the model; disordering of $\alpha5$–$\alpha6$ has also been observed in other structures of BTB-domain fragments that lack the BTB N-terminus (for example, KBTBD4; PDB entry 2eqx; RIKEN Structural Genomics/Proteomics Initiative, unpublished work). The SPOP C-terminal domain (CTD; residues 296–359) comprises five α-helices, denoted $\alpha7$–$\alpha11$, with $\alpha11$ residues contributing most of the interactions at the dimerization interface. The dimer interface buries 685 Å² of surface area per monomer and is stabilized by hydrogen-bond interactions between Tyr353 and Asn326′ and between Arg354 and Glu334′, together with a salt bridge between Arg354 and Glu334′. The dimer interface and the $\alpha9$–$\alpha10$–$\alpha11$ fold are stabilized by the burial of hydrophobic residues that include Val349, Ala350, Ala352, Leu356 and Ala357.

To confirm the role of the $\alpha11$ residues in the high-order oligomerization of SPOP, we purified proteins that contained the entire BTB domain together with various parts of the C-terminus. SPOP[169–359], which contains an intact CTD but

lacks the predicted NLS, eluted as a high-molecular-weight species upon size-exclusion chromatography and the purified protein could be cross-linked into a high-order oligomer; in contrast, SPOP proteins that had truncations in $\alpha11$ (SPOP[169–344] and SPOP[169–355]) were dimeric (Supplementary Fig. 1*c*). The high-order oligomerization of SPOP is thus mediated by two independent self-association interfaces: the classic BTB dimerization interface and the dimerization interface of the CTD.

3.2. Organization of the SPOP BTB and C-terminal domains

BTB-domain dimers are domain-swapped dimers that have very low dissociation constants ($K_d < 200$ n*M*; Li *et al.*, 1997), whereas oligomerization directed by the SPOP C-terminus is dynamic and dissociable in solution (Errington *et al.*, 2012). In order to obtain protein crystals of the contiguous SPOP BTB and CTD domains in a single molecule, we therefore attempted to disrupt CTD dimerization by point mutation of an interface residue. We mutated Tyr353 to glutamic acid in the context of the SPOP[169–374] protein that contained an intact BTB and CTD. In contrast to the high-order oligomerization observed with SPOP[169–374], SPOP[169–374 Y353E] was dimeric when analysed by size-exclusion chromatography, and the purified protein could be cross-linked into a dimer

(Supplementary Fig. S1d), confirming the role of Tyr353 in CTD dimerization and in high-order oligomerization.

We determined the X-ray crystal structure of SPOP[169–374 Y353E] at 2.4 Å resolution (Table 1 and Fig. 2a). SPOP[169–374 Y353E] crystallized as a BTB-mediated dimer; there were no inter-actions between the CTD residues of neighbouring SPOP molecules in the crystal, consistent with the complete disruption of the CTD dimerization interface in the SPOP Y353E mutant. Residues 177–329 of SPOP[169–374 Y353E] superposed extremely well (r.m.s.d. value of 0.49 Å for C^α-atom positions) with a reported SPOP structure (PDB entry 3htm; SPOP residues 177–329; Zhuang et al., 2009) that contains the classic BTB domain (α1–α6; residues 177–296) together with the helical hairpin (α7–α8; residues 300–327) that was dubbed the 3-box (Zhuang et al., 2009). Additionally, residues 300–356 of SPOP[169–374 Y353E] superposed extremely well with SPOP[270–374 L273D L282D L285K] (r.m.s.d. value of 0.46 Å for C^α-atom positions; Fig. 3a), suggesting that the relative orientation of the SPOP CTD and BTB domains is inflexible. No electron density was observed for residues 169–176 and 357–374 of SPOP[169–374 Y353E], and residues comprising the α3–β4 loop were associated with higher crystallographic B factors, as reported previously (Zhuang et al., 2009; Errington et al., 2012).

The α7–α8 hairpin of the SPOP CTD interacts with the α5–α6 helices of the BTB domain to form an antiparallel four-helix bundle, whereas the CTD helices α9–α10–α11 form a distinct motif that lies perpendicular to α7–α8. The overall fold of the SPOP CTD resembles the N-terminal portion of the 130-residue α-helical BACK (**B**TB **a**nd **C**-terminal **K**elch) domain that is found C-terminal to the BTB domain in the Kelch-type Cul3 adaptors (Stogios & Privé, 2004). The struc-ture of SPOP[169–374 Y353E] superposed well (r.m.s.d value of 2.48 Å for C^α-atom positions) with the contiguous BTB and BACK domains of the Kelch-type BTB adaptor KLHL11 (PDB entry 3i3n; Canning et al., 2013), with the relative orientation of the BTB and BACK domains being conserved between the two proteins (Fig. 2b). The residues preceding α1 of the BTB domain are oriented differently in SPOP and KLHL11, and interact with different regions of the opposite chain in the domain-swapped dimer, as reported previously (Canning et al., 2013; Errington et al., 2012).

3.3. Model of the high-order SPOP oligomer

We generated a model of the high-order SPOP oligomer by iterative superposition of the dimeric SPOP[169–374 Y353E] and SPOP[270–374 L273D L282D L285K] structures that contain the BTB- and CTD-interaction interfaces, respectively (Fig. 3a). We also modelled the substrate-recruiting MATH domains using an available SPOP structure (PDB entry 3hqi; Zhuang et al., 2009). The model of the high-order SPOP oligomer depicts alternating BTB and CTD dimers assembled in a left-handed helical manner that reflects the skewed arrangement of the constituent twofold-symmetry axes (Figs. 3a and 3b). Although the extent of high-order oligomerization in vivo is not known, a full turn of the SPOP helix would contain approximately 16

SPOP chains (eight BTB and eight CTD dimers) and have a pitch of 510 Å. The SPOP MATH domains are flexibly tethered to the BTB domain (Zhuang et al., 2009) and are organized in a contiguous array along one face of the oligomer. To confirm the model of the high-order SPOP oligomer, we visualized the SPOP[169–374] complex using atomic force microscopy (AFM). AFM images depict a linear organization of the subunits of the SPOP oligomer; most of the molecules have a curved or horseshoe shape, consistent with a helical structure that has broken and kinked during the sequential deposition of its subunits onto the grid (Fig. 3c and Supplementary Fig. S3).

We also modelled a high-order oligomer of the SPOP E3 ligase complex that contains Cul3 and the E2-binding RING protein RBX1 (Fig. 3d). This model was generated by super-position using common regions from available structures: the
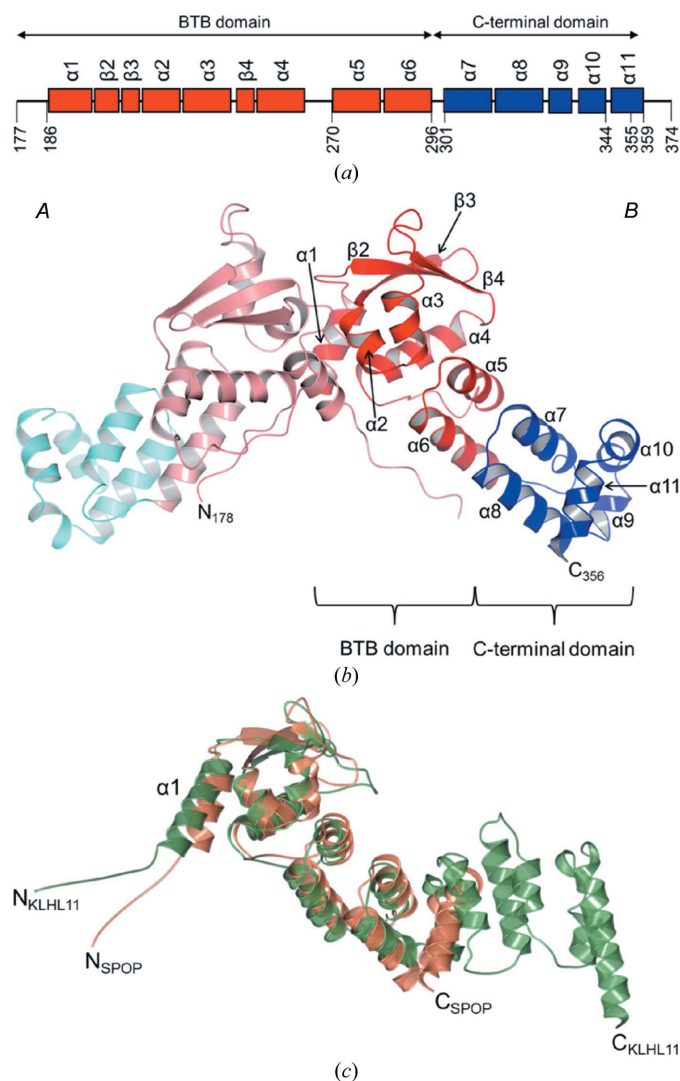

Figure 2
Organization of the SPOP BTB and C-terminal domains. (a) Crystal structure of the SPOP[169–374 Y353E] dimer. BTB domains are coloured red and pink; CTDs are coloured blue and cyan. Secondary-structure elements of the B chain are indicated. (b) Superposition of SPOP[169–374 Y353E] (orange) with the BTB and BACK domains of KLHL11 (PDB entry 3i3n; green).

first two cullin repeats were from SPOP^{BTB}–Cul3 (PDB entry 4eoz; Errington *et al.*, 2012) and the third cullin repeat and the cullin C-terminal domain together with RBX1 were from Cul1–RBX1 (PDB entry 1ldj; Zheng *et al.*, 2002). The model of the high-order SPOP oligomer is compatible with the recruitment of a Cul3 molecule to each SPOP chain without creating steric clashes. The model suggests that the N-terminus of Cul3 interacts with residues from both the BTB and CTD domains of SPOP, consistent with a recent structure that revealed the interaction of Cul3 with both the BTB and BACK domains of KLHL11 (PDB entry 4ap2; Canning *et al.*, 2013); the relative orientation of the BTB and Cul3 molecules is identical in the KLHL11–Cul3 and SPOP–Cul3 structures (PDB entries 4ap2 and 4eoz, respectively). The elongated Cul3 molecules extend in arcs away from the SPOP BTB-CTD backbone to form two rows of arms that bend towards the inner curve of the helix. The RBX1 molecules that interact with the C-termini of the cullins to recruit the E2-conjugating enzyme are thus arranged in two rows that flank the central MATH domains on the same face of the assembly.

4. Discussion

The model of the high-order SPOP–Cul3–RBX1 oligomer provides insight into the possible mechanisms whereby adaptor oligomerization regulates substrate ubiquitination. The α-helical core of the contiguous SPOP CTD and BTB domains forms a rigid framework upon which multiple β-sheet MATH domains are flexibly tethered along one face. This arrangement of MATH domains could enhance the efficiency and versatility of substrate recruitment by increasing the rate of binding and by facilitating simultaneous interactions with multiple degrons that might be variably positioned within
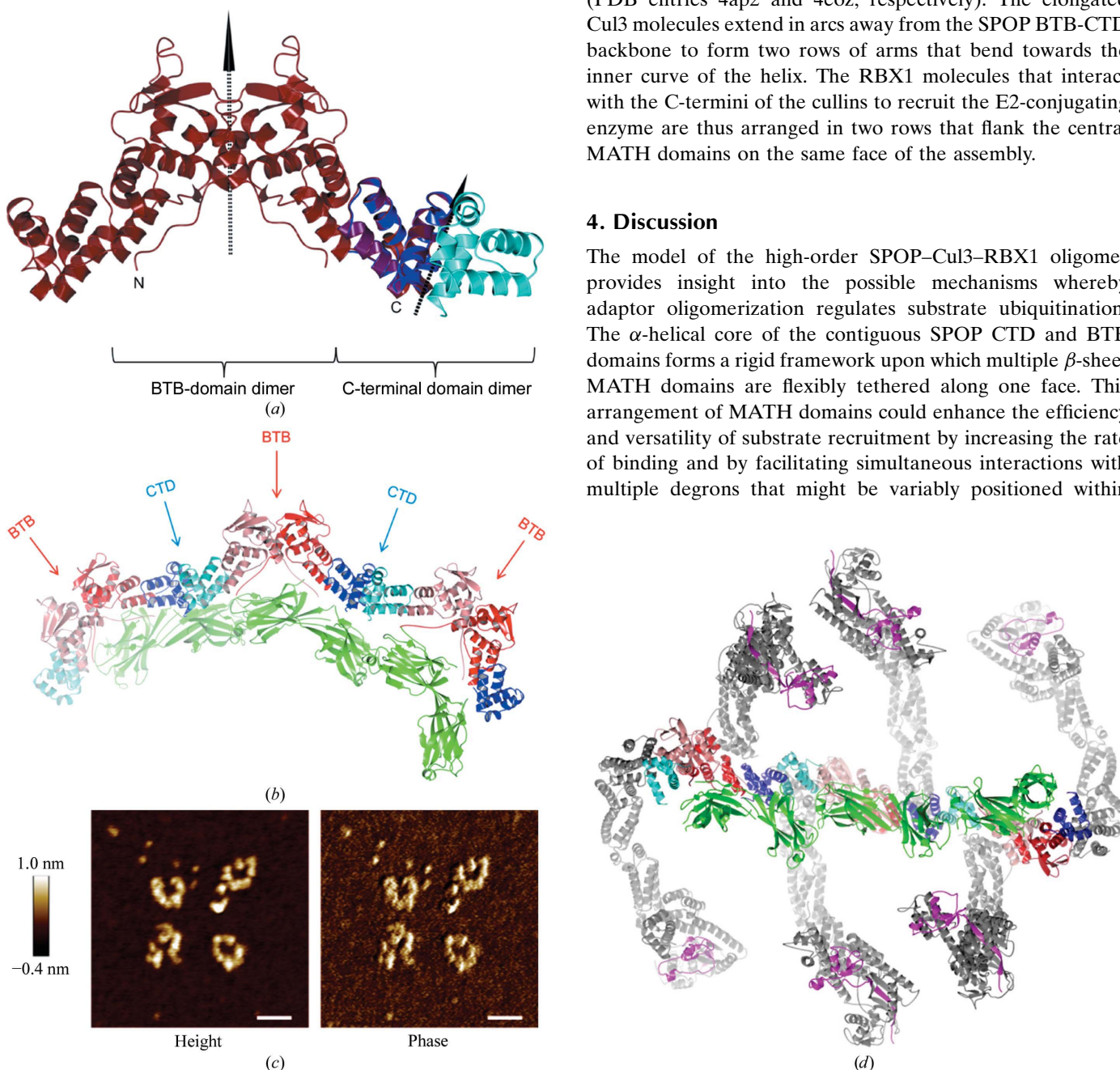

Figure 3
High-order SPOP oligomers. (*a*) Superposition of the SPOP CTD dimer (blue and cyan) with the SPOP$^{169–374\ Y353E}$ dimer (brown). The rotation axes of the CTD and BTB domains are indicated. (*b*) Model of a high-order SPOP oligomer. The model depicts six SPOP molecules and was generated by iterative superposition of the SPOP CTD dimer with the SPOP$^{169–374\ Y353E}$ dimer using structural alignment of the common α7–α10 residues (300–344). BTB domains are coloured red and pink; CTDs are coloured blue and cyan. The SPOP MATH domains (residues 28–166; green) that recruit substrates for ubiquitination were modelled by superposition from the SPOP$^{BTB+MATH}$ structure (PDB entry 3hqi). (*c*) AFM images of SPOP$^{169–374}$ oligomers. A representative example is shown. The scale bar corresponds to 50 nm. (*d*) Model of a high-order SPOP–Cul3–RBX1 complex. The SPOP oligomer was used as a template on which Cul3 and RBX1 were modelled. The first two cullin repeats of the Cul3 N-terminal domain were modelled using the structure of SPOP^{BTB}–Cul3 (PDB entry 4eoz); the third cullin repeat, the cullin C-terminal domain and RBX1 were modelled using the structure of Cul1–RBX1 (PDB entry 1ldj). Cullin chains are coloured grey and RBX1 chains are coloured magenta.

a single substrate molecule; such cooperative multivalent interactions would be particularly important in the recognition of substrates with multiple weak degrons (Zhang *et al.*, 2009; Zhuang *et al.*, 2009). The high-order oligomerization of SPOP would also result in the concentration of multiple E2 conjugating enzyme molecules close to the substrate on the same face of the assembly, thereby increasing the rate of the ubiquitination reaction.

The mechanisms that modulate the oligomeric state of SPOP *in vivo* remain to be determined, although it is feasible that such regulation might provide a mechanism for the differential ubiquitination of individual substrates according to the number and strength of the degrons that they contain. It has been reported that the SPOP C-terminal region is required for the ubiquitination and degradation of the substrate Daxx in transfected mammalian cells (Kwon *et al.*, 2006), consistent with the importance of high-order oligomerization *in vivo*. The human genome encodes a closely related SPOP paralogue, SPOPL (Choo *et al.*, 2010), that interacts both with SPOP substrates and with Cul3 *in vitro* (Errington *et al.*, 2012) and is highly conserved among vertebrates. The BTB domains of SPOP and SPOPL are 87% identical and the two proteins form BTB-mediated heterodimers *in vitro*; in contrast, the SPOP and SPOPL CTDs differ, with the SPOPL CTD containing an 18-residue insertion that prevents high-order oligomerization (Errington *et al.*, 2012). SPOPL restricts the high-order oligomerization of SPOP in mixtures of the two proteins *in vitro*; this results from the formation of BTB-mediated hetero-oligomers and it has therefore been speculated that the relative levels of SPOP and SPOPL *in vivo* might determine the degree of SPOP oligomerization (Errington *et al.*, 2012). The dimerization interface of the SPOP CTD buries a relatively small surface area and can be completely disrupted by the mutation of Tyr353 to glutamic acid; it is therefore highly suited for directing the dynamic high-order association of the more stable BTB-mediated SPOP dimers and it will be relevant to determine whether oligomerization is regulated by the phosphorylation of Tyr353 *in vivo*.

The SPOP CTD resembles the N-terminal portion of the α-helical BACK domain that is found C-terminal to the BTB domain in the Kelch-type Cul3 adaptors. It is predicted that Cul3 interacts with the SPOP CTD in a manner that resembles its interaction with the BACK domain of the Kelch-type adaptor KLHL11, and the relative orientation of the BTB and Cul3 molecules is identical in SPOP–Cul3 and KLHL11–Cul3. It is not known whether the BACK domain mediates high-order oligomerization of the BTB Kelch-type adaptors: the Kelch-type adaptors Keap1 and gigaxonin have been reported as BTB-mediated dimers (Ogura *et al.*, 2010; Zhuang *et al.*, 2009) and crystal structures of BACK domains have not thus far revealed self-interaction interfaces (PDB entries 3hve, 2eqx and 3i3n). Thus, although the BTB-mediated SPOP–Cul3 and KLHL11–Cul3 dimers have a similar architecture, the SPOP CTD may represent a truncated BACK domain that has evolved an additional specialized function in high-order oligomerization; it is feasible that differences in the oligo-

merization properties of the individual BTB MATH-type and Kelch-type Cul3 adaptors have evolved alongside differences in the modes of substrate recognition and of regulation.

Protein self-assembly provides both architectural and regulatory roles in biological systems, and high-order oligomerization is a feature of proteins that contain more than one distinct self-association domain. For example, the two independent self-association interfaces of the centriole protein, SAS-6, direct its assembly into a cartwheel structure with ninefold symmetry that forms the basis of the centriolar core (Kitagawa *et al.*, 2011). The high-order oligomerization of BTB-domain proteins has been well documented, although the structural basis for these associations has thus far remained elusive. The model of the high-order SPOP oligomer described here provides a structural basis for the regulation of substrate ubiquitination by adaptor oligomerization; this will be relevant for understanding the control of ubiquitination and may direct the rational design of inhibitors for use in the therapeutic targeting of ubiquitination complexes.

References

Barbieri, C. E. *et al.* (2012). *Nature Genet.* **44**, 685–689.

Canning, P., Cooper, C. D., Krojer, T., Murray, J. W., Pike, A. C., Chaikuad, A., Keates, T., Thangaratnarajah, C., Hojzan, V., Marsden, B. D., Gileadi, O., Knapp, S., von Delft, F. & Bullock, A. N. (2013). *J. Biol. Chem.* **288**, 7803–7814.

Choo, K.-B., Chuang, T.-J., Lin, W.-Y., Chang, C.-M., Tsai, Y.-H. & Huang, C.-J. (2010). *Gene*, **460**, 39–47.

Cohen, S. X., Ben Jelloul, M., Long, F., Vagin, A., Knipscheer, P., Lebbink, J., Sixma, T. K., Lamzin, V. S., Murshudov, G. N. & Perrakis, A. (2008). *Acta Cryst.* D**64**, 49–60.

Chen, V. B., Arendall, W. B., Headd, J. J., Keedy, D. A., Immormino, R. M., Kapral, G. J., Murray, L. W., Richardson, J. S. & Richardson, D. C. (2010). *Acta Cryst.* D**66**, 12–21.

Emsley, P., Lohkamp, B., Scott, W. G. & Cowtan, K. (2010). *Acta Cryst.* D**66**, 486–501.

Errington, W. J., Khan, M. Q., Bueler, S. A., Rubinstein, J. L., Chakrabartty, A. & Privé, G. G. (2012). *Structure*, **20**, 1141–1153.

Espinás, M. L., Jiménez-García, E., Vaquero, A., Canudas, S., Bernués, J. & Azorín, F. (1999). *J. Biol. Chem.* **274**, 16461–16469.

Evans, P. (2006). *Acta Cryst.* D**62**, 72–82.

Kabsch, W. (2010). *Acta Cryst.* D**66**, 125–132.

Kim, B., Nam, H. J., Pyo, K. E., Jang, M. J., Kim, I. S., Kim, D., Boo, K., Lee, S. H., Yoon, J.-B., Baek, S. H. & Kim, J. H. (2011). *Biochem. Biophys. Res. Commun.* **415**, 720–726.

Kitagawa, D., Vakonakis, I., Olieric, N., Hilbert, M., Keller, D., Olieric, V., Bortfeld, M., Erat, M. C., Flückiger, I., Gönczy, P. & Steinmetz, M. O. (2011). *Cell*, **144**, 364–375.

Komander, D. & Rape, M. (2012). *Annu. Rev. Biochem.* **81**, 203–229.

Krissinel, E. & Henrick, K. (2007). *J. Mol. Biol.* **372**, 774–797.

Kwon, J. E., La, M., Oh, K. H., Oh, Y. M., Kim, G. R., Seol, J. H., Baek, S. H., Chiba, T., Tanaka, K., Bang, O. S., Joe, C. O. & Chung, C. H. (2006). *J. Biol. Chem.* **281**, 12664–12672.

Li, C., Ao, J., Fu, J., Lee, D.-F., Xu, J., Lonard, D. & O'Malley, B. W. (2011). *Oncogene*, **30**, 4350–4364.

Li, X., Lopez-Guisa, J. M., Ninan, N., Weiner, E. J., Rauscher, F. J. III & Marmorstein, R. (1997). *J. Biol. Chem.* **272**, 27324–27329.

Liu, J. *et al.* (2009). *Science*, **323**, 1218–1222.

Maiti, R., Van Domselaar, G. H., Zhang, H. & Wishart, D. S. (2004). *Nucleic Acids Res.* **32**, W590–W594.

McCoy, A. J., Grosse-Kunstleve, R. W., Adams, P. D., Winn, M. D., Storoni, L. C. & Read, R. J. (2007). *J. Appl. Cryst.* **40**, 658–674.

McNicholas, S., Potterton, E., Wilson, K. S. & Noble, M. E. M. (2011). *Acta Cryst.* D**67**, 386–394.

Murshudov, G. N., Skubák, P., Lebedev, A. A., Pannu, N. S., Steiner, R. A., Nicholls, R. A., Winn, M. D., Long, F. & Vagin, A. A. (2011). *Acta Cryst.* D**67**, 355–367.

Nagai, Y., Kojima, T., Muro, Y., Hachiya, T., Nishizawa, Y., Wakabayashi, T. & Hagiwara, M. (1997). *FEBS Lett.* **418**, 23–26.

Nalepa, G., Rolfe, M. & Harper, J. W. (2006). *Nature Rev. Drug Discov.* **5**, 596–613.

Ogura, T., Tong, K. I., Mio, K., Maruyama, Y., Kurokawa, H., Sato, C. & Yamamoto, M. (2010). *Proc. Natl Acad. Sci. USA*, **107**, 2842–2847.

Petroski, M. D. (2008). *BMC Biochem.* **9**, S7.

Pintard, L., Willems, A. & Peter, M. (2004). *EMBO J.* **23**, 1681–1687.

Schneider, T. R. & Sheldrick, G. M. (2002). *Acta Cryst.* D**58**, 1772–1779.

Sheldrick, G. M. (2008). *Acta Cryst.* A**64**, 112–122.

Stogios, P. J., Downs, G. S., Jauhal, J. J., Nandra, S. K. & Privé, G. G. (2005). *Genome Biol.* **6**, R82.

Stogios, P. J. & Privé, G. G. (2004). *Trends Biochem. Sci.* **29**, 634–637.

Takahashi, I., Kameoka, Y. & Hashimoto, K. (2002). *Biochim. Biophys. Acta*, **1591**, 63–68.

Winter, G. (2010). *J. Appl. Cryst.* **43**, 186–190.

Zhang, K. Y. J., Cowtan, K. & Main, P. (1997). *Methods Enzymol.* **277**, 53–64.

Zhang, Q., Shi, Q., Chen, Y., Yue, T., Li, S., Wang, B. & Jiang, J. (2009). *Proc. Natl Acad. Sci. USA*, **106**, 21191–21196.

Zheng, N., Schulman, B. A., Song, L., Miller, J. J., Jeffrey, P. D., Wang, P., Chu, C., Koepp, D. M., Elledge, S. J., Pagano, M., Conaway, R. C., Conaway, J. W., Harper, J. W. & Pavletich, N. P. (2002). *Nature (London)*, **416**, 703–709.

Zhuang, M., Calabrese, M. F., Liu, J., Waddell, M. B., Nourse, A., Hammel, M., Miller, D. J., Walden, H., Duda, D. M., Seyedin, S. N., Hoggard, T., Harper, J. W., White, K. P. & Schulman, B. A. (2009). *Mol. Cell*, **36**, 39–50.

Zimmerman, E. S., Schulman, B. A. & Zheng, N. (2010). *Curr. Opin. Struct. Biol.* **20**, 714–721.